High Precision Implicit Modeling for Patient-Specific Coronary Arteries

QINGQI HONG[1], QINGDE LI[2], BEIZHAN WANG[1], KUNHONG LIU[1], AND QUAN QI[3]
[1]Software School, Xiamen University, Xiamen 361005, China
[2]School of Engineering and Computer Science, University of Hull, Hull HU6 7RX, U.K.
[3]College of Information Science and Technology, Shihezi University, Shihezi 832007, China

Corresponding author: Kunhong Liu (lkhqz@xmu.edu.cn)

ABSTRACT High precision geometric reconstruction of patient-specific coronary arteries plays a crucial role in visual diagnosis, treatment decision-making, and the evaluation of the therapeutic effect of interventions in coronary artery diseases. It is also a fundamental task and a basic requirement in the numerical simulation of coronary blood flow dynamics. In this paper, a new implicit modeling technique for the geometric reconstruction of patient-specific coronary arteries has been developed. In the proposed method, the coronary arteries geometry is reconstructed segment by segment using radial basis functions with ellipsoid constraint from the point cloud obtained with a volumetric vascular image segmentation method, and the individually reconstructed coronary branches are then combined using a shape-preserving implicit blending operation to form a complete coronary artery surface. The experiment results and validations indicate that the reconstructed vascular shapes are of high smoothness and faithfulness.

INDEX TERMS Coronary arteries, implicit modeling, vascular visualization.

I. INTRODUCTION

Coronary Artery Disease (CAD) is recognized as one of the three world's most deadly diseases that seriously threaten human life and health [1]. CAD is caused by coronary atherosclerosis luminal stenosis or occlusion, and can lead to myocardial ischemia, hypoxia, or myocardial infarction. Nowadays the gold standard in the diagnosis of CAD is the routine clinical catheter coronary angiography, which can provide accurate information about the location, quantity and severity of coronary stenosis. However, the cost of coronary angiography examination is high, which can reach up to several hundred dollars [2]. What is more, the examination involves a certain degree of invasiveness and can lead to high risk of injury to patients, of which mortality is about 0.15% and morbidity is about 1.5% [3]. With the rapid development of Computer Tomography (CT) technology, current Electrocardiogram (ECG) -gated control technology based heart coronary Computed Tomography Angiography (CTA) has now been able to provide multi-temporal three-dimensional images of heart and coronary arteries with high resolution, which can clearly display the coronary artery lumen,

calcified plaque, and other information. Coronary CTA has the advantages of noninvasive, fast check, and low cost, and has become a promising way of imaging for the evaluation of CAD.

At present, the main task of computer processing for coronary CTA images is the 3-D visualization of coronary arteries, which utilizes the direct volume rendering method to generate three-dimensional stereo images from a series of two-dimensional slices. Compared with two-dimensional slices, the generated stereo images can help doctors to intuitively visualize the location and size of lesions, and its spatial relationship with surrounding tissues, which thus greatly improves the accuracy of diagnosis. However, just to be able to visualize the hidden human tissues and structures is far from sufficient, which is especially the case when a certain numerical simulation is required to assess the possible outcomes of a planned treatment. In fact, the availability of highly accurate geometric information of human tissues is an essential and fundamental task in many clinical applications. For example, a precise geometric representation of a vasculature can not only provide doctors with more accurate visual information regarding the vascular topology and surface details, but, more importantly, can be applied directly to solve various problems concerning vascular surface analysis,

The associate editor coordinating the review of this manuscript and approving it for publication was Orazio Gambino.

such as the calculation of vascular surface curvature and shear stress. It helps doctors make more accurate diagnosis and more reasonable surgical planning for treatment of vascular diseases. Compared with a simple visualization, the accurate reconstruction of patient-specific geometric models of coronary arteries from CTA images will play a greater advantage in many aspects. For instance, the accurate geometry reconstruction of patient-specific coronary model is the primary step for the numerical simulation of coronary blood flow dynamics. Many studies have shown that, the analysis of vascular hemodynamic has important clinical values for the forecast, diagnosis, and the evaluation of the prognosis of atherosclerosis. In addition, it would be much easier to design and evaluate possible modification of patient-specific artery model, when there is an explicit geometry representation for the coronary artery structure. Simulations of the coronary blood flow based on the modified geometry models enable the study of hemodynamic characteristics, which is very helpful to choose the optimal interventional procedures (i.e. stenting or bypass grafting) for treating CAD.

In this paper, we develop a new implicit modeling technique for the geometric reconstruction of coronary arteries. In the proposed method, the vascular surface is reconstructed segment by segment using Radial Basis Functions with Ellipsoid Constraint (RBFEC) [6] from the point cloud obtained with a volumetric vascular image segmentation method. Then, the Smooth Piecewise Polynomial Blending Operator (SPPBO) [7], a shape-preserving implicit surface blending operator, is employed to blend different implicitly-defined vascular segments to form a complete vessel branch, which is further to be combined with other implicitly reconstructed vascular branches, again, using SPPBO. The proposed methods have been applied to plenty of coronary arteries CTA images and other medical datasets, and the experiment results show that the reconstructed vascular shapes are of high smoothness and accuracy. We also perform the qualitative analysis and quantitative comparison with other methods to validate the proposed techniques.

II. RELATED WORK

Generally, there are two main steps for the geometry reconstruction of vascular structures: image segmentation and surface modeling [4]. A large number of segmentation techniques have been developed for solving various image segmentation problems. However, due to the high complexity of vascular structures, it is still a tough job to segment the vascular region from initial vessel images [8]. Interested readers can refer to [8] for a relatively thorough review on the vascular segmentation techniques.

Currently, several specific techniques have been proposed to address the issue of coronary artery segmentation, including region growing based method [9], active contour model based method [10], pattern recognition based methods [11], [12]. However, extracting the geometry of the coronary arteries robustly and with high precision remains a tough issue, as the coronary arteries have very thin

geometries and the corresponding coronary images usually contain very high amount of noise (i.e. plaques with various morphology) [11].

Once the segmentation result is obtained, it is usually expressed as polygonal meshes or a discrete point set. However, the visualization and analysis directly based on raw segmentation data is prone to errors and not appropriate in the clinical applications, such as numerical simulation of blood flow dynamics, vascular surgery planning, computer aided vascular surgery, and so on. Thus, it is necessary and essential to employ geometry modeling techniques to reconstruct a continuous and solid geometry of vasculatures. According to the way of representing a geometric surface, the approaches for modeling vascular geometry can be categorized into two groups: explicit methods and implicit methods. The explicit modeling method represents a vascular surface with polygon meshes or parametric functions, which is relatively mature. Various explicit modeling approaches have been developed for the geometric reconstruction of vasculatures, as the purpose of geometric modeling is mainly on vascular structure visualization. A representative example of explicit method is to utilize simple parametric geometric primitives (i.e. truncated cones [13], cylinders [14]) to represent the vascular surfaces. Several advanced explicit modeling techniques have been suggested to construct vascular shapes based on vascular skeleton structures [15]–[18]. However, in the explicit method, it is a difficult task to perform shape blending operations and bifurcations, since the underlying geometric shapes are expressed as parametric surfaces or triangle meshes [19]. In addition, as the explicitly represented vascular surface does not provide direct information on which side of the reconstructed surface corresponds to the inside of the vasculatures, relevant collision detection algorithms for explicitly represented vessel surfaces are usually very complex.

The other way is the implicit modeling method, which represents the underlying geometric shape of vasculatures as implicit functions, such as the implicit modeling techniques developed in Bloomenthal's work [19]. Generally, implicit modeling method has several advantages over explicit method. For instance, an implicit function can be viewed both as a surface and a volumetric solid, and different implicitly represented geometric objects can be easily blended together in various ways [7], [20]. In addition, it would be much easier to implement the collision detection operation based on the implicitly represented objects, since the implicit function value at a point can directly indicate whether a point lies inside or outside the objects [21]. Consequently, several implicit modeling techniques have developed for the geometry reconstruction of vasculatures. Oeltze and Preim [22] presented a method for visualizing vasculature based on Convolution Surfaces (CS) [23], which can achieve excellent visualization result of vessel structures. However, the CS technique only represents vasculature with a morphological approximation, which is unable to faithfully reconstruct the vascular structures with pathology. In order to represent the vessel structures more accurately, Schumann *et al.* [24], [25]

presented a model-free visualization method based on Multi-level Partition of Unity Implicits (MPUI) [26]. However, the MPUI method is not robust to recover fine details from noisy data, and the quality of the resulting surfaces is not good enough in terms of fitting accuracy and the smoothness of the fitted surface [27]. In order to achieve better results, Hong *et al.* [28]–[31] developed sweep surface based methods for the reconstruction of vascular geometry, which specify vessel cross sections using 2D Piecewise Algebraic Splines (PAS) [32] or 2D radial basis functions [6]. Another implicit modeling method based on sweep surfaces has been developed in Kretschmer *et al.*'s work [33] to achieve high-quality vascular structures. Although the sweep surface based methods can reconstruct vasculatures with high smoothness, the modeling accuracy could be affected in the case of much curved centerline. Recently, a Local Implicit Modeling (LIM) algorithm is developed by Kerrien *et al.* [34] for blood vessel modeling, with a more efficient energy formulation and a more discriminative blob selection criterion.

III. GEOMETRY RECONSTRUCTION OF CORONARY ARTERIES

The structure of human vascular system is quite similar to the tree structure in natural world, which is intricate and complex but also has a certain regularity. In the following, a tree-like shape modeling technique based on RBFEC will be proposed and applied to the geometry reconstruction of coronary arteries.

A. TREE-LIKE SHAPE MODELING BASED ON RBFEC

In the proposed tree-like shape modeling technique, the discrete contour points extracted from a vascular surface with an image segmentation technique is firstly grouped according to tree branches. For each tree-branch, the corresponding point cloud is further subdivided into a set of smaller point clouds, each of which corresponds to a smaller vascular segment. An implicit surface is then fitted to each sub-point cloud using an implicit surface fitting technique known as Radial Basis Functions with Ellipsoid Constraint (RBFEC). A set of implicit surfaces created along each branch during the process is then combined together to construct a long tubular implicit shape corresponding to the entire branch using a shape-preserving implicit blending operation, called, Smooth Piecewise Polynomial Blending Operator (SPPBO); finally, the implicitly defined shapes of different branches are further blended together, again, using SPPBO, to construct the overall implicit surfaces corresponding to the entire tree structure.

RBFEC was introduced by Li *et al.* [6] for the purpose of implicit surface fitting. The RBFEC fitting technique does not need to use information about surface normal but still can fit the data accurately when the underlying geometry captured by the point cloud is relatively simple. The tubular shape modeling method is developed based on this idea, as a curved tubular is almost cylindrical when it is cut into short segments. In addition, unlike most implicit fitting techniques, where the point cloud to be fitted is usually assumed to have
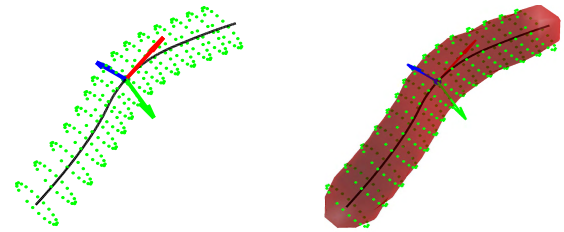
FIGURE 1. The sub-point cloud (left), and the constructed tubular shape segment from the sub-point cloud by using the Radial Basis Functions with Ellipsoid Constraint (right).

a high density, RBFEC can produce a relatively meaningful fitting when the data points provided are sparse or even with big holes.

In this section, we propose an implicit tubular shape modeling method by fitting an implicit function expressed in a form of RBFEC to a point cloud $\mathcal{P}$ sampled from the surface of a tubular object with a known skeleton. Let the skeleton of a tubular object be represented as a B-spline curve $S(s)$ along parameter s. The method is described as follows:

1) Subdivide the tubular skeleton into a collection of segments corresponding to $s = s_0, s_1, \cdots, \cdots, s_{N-1}$. The length of the subdivided tubular segment l_s is indicated by the number of the interpolated-spline points of the parametric skeleton $S(s)$, which is generally defined to be in inverse proportion to the accumulated curvature and torsion of the skeleton segment.

2) Let the point cloud be $\mathcal{P} = \{P_k, k = 0, 1, \cdots, K-1\}$. Divide the point cloud into a collection of smaller point sets based on the skeleton segments generated in the last step:

$$\mathcal{P}_i = \{P_{ij}, j = 0, 1, \cdots, N_i\}, \quad i = 0, 1, \cdots, N-1$$

where $\mathcal{P}_i$ is the sub-point cloud corresponding to the *i*-th tubular segment (see Fig.1 (left)).

3) For each sub-point cloud $\mathcal{P}_i$, fit an implicit surface to $\mathcal{P}_i$ using RBFEC. Let $P(x, y, z)$ represent a general point in 3-D space, then the implicitly fitted surface for point cloud $\mathcal{P}_i$ using RBFEC can be expressed directly in the following way:

$$F_i(P) = \sum_{j=1}^{N_i} \lambda_{ij} \Phi_{ij}(\|P - P_{ij}\|) + \rho(P) = 0 \quad (1)$$

where λ_{ij} is the coefficient, $\Phi_{ij}(\cdot)$ is the radial basis function corresponding to position P_{ij}, and $\rho(\cdot)$ is the ellipsoid constraint polynomial part defined in [6]. Fig.1 (right) shows the constructed tubular shape segment from a sub-point cloud by using RBFEC.

4) Blend the collection of implicit surfaces $F_0, F_1, \cdots, F_{N-1}$ obtained in step (3) using SPPBO to obtain a complete implicit surface corresponding to the entire tubular skeleton.

It should be noted that classifying the points sampled from a highly curved tubular object into smaller point sets and

then fit the tubular surface piece by piece is necessary, as the fitting results can be very inaccurate when fitting the entire tubular surface as one step fitting using RBFEC. In addition, a proper implicit blending operator is required to combine the set of implicit surfaces reconstructed locally corresponding to each sub-point cloud. In this paper, we employ the Smooth Piecewise Polynomial Blending Operator (SPPBO) to do the shape-blending task. The main reason to use SPPBO is that SPPBO is a kind of shape-preserving blending operation, which allows the original shapes involved in the blending process to be preserved up to a specified accuracy. SPPBO is defined using the smooth absolute function, which can be expressed either explicitly or implicitly as an iterative process. The explicit form of the C^n continuous absolute function can be expressed directly as a formula shown below:

$$|x|_0 = |x|$$

$$|x|_n = \frac{1}{(n+1)!2^n} \sum_{k=0}^{n-1} (-1)^k \binom{n-1}{k} G_n(x+n-2k-1) \quad (2)$$

where

$$G_n(x) = (x+1)^n |x+1| - (x-1)^n |x-1|,$$
$$n = 1, 2, \cdots .$$

With the smooth absolute function, the C^n SPPBO $\max_{n,\delta}(x, y)$ is defined in the following form [7]:

$$\max_{n,\delta}(x, y) = \frac{1}{2}(x + y + |x - y|_{n,\delta}) \quad (3)$$

where

$$|x|_{n,\delta} = \frac{\delta}{n} \left| \frac{nx}{\delta} \right|_n .$$

For implicit surfaces $F_0, F_1, \cdots, F_{N-1}$ obtained in step (3) corresponding to all the skeleton segments, the implicit function corresponding to the entire tabular skeleton can be achieved by blending all these implicit functions using $\max_{n,\delta}(x, y)$:

$$F_{blend} = F_0;$$
$$for\ i = 1\ to\ N - 1$$
$$F_{blend} = \max_{n,\delta}(F_{blend}, F_i). \quad (4)$$

Fig.2 demonstrates the smooth blending of three implicitly defined shapes to form a complete tubular shape. The left to middle-right sub-figures represent three individual implicit objects, and the right sub-figure represents the blending result of these three objects by using the SPPBO.

Once implicit surfaces corresponding to different tubular branches of a tree structure have been built by following the steps (1) to (4), these implicit surfaces can be further combined together, again, using SPPBO. Fig.3 demonstrates the smooth blending of two implicitly reconstructed tubular surfaces. The left and the middle sub-figures represent two
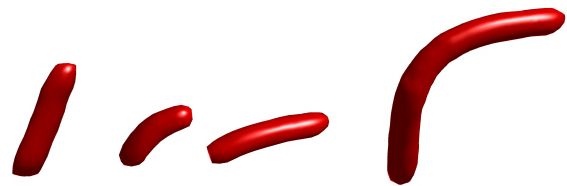

FIGURE 2. The smooth blending of three implicitly defined shapes (from left to middle right) to form a complete tubular shape (right).
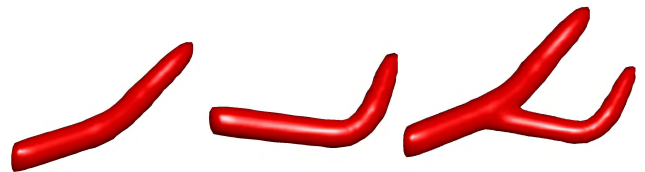

FIGURE 3. The smooth blending of two implicitly reconstructed tubular surfaces by using SPPBO.

individual branching models, and the right sub-figure represents the blending result of these two models by using SPPBO.

It is worth noting that the method described above can be directly used as an implicit tree-like object modeling technique. This is because, by using this method, any parametrically described tubular objects, such as those modelled with extrusion and various spline techniques, can be directly re-represented in implicit form approximately with any required accuracy.

B. GEOMETRY RECONSTRUCTION OF CORONARY ARTERIES BASED ON RBFEC

In this section, we apply the method proposed above to the accurate geometry reconstruction of coronary arteries. Fig.4 presents the pipeline, and the main steps are described as follows:

1) Extract coronary artery skeleton from the segmented volumetric coronary artery image.
2) For a given vessel branch, divide its skeleton into a sequence of short skeleton segments, and for each skeleton segment, compute an Axis-Aligned Bounding Box (AABB) in voxel coordinates that contains the vessel segment.
3) In this AABB volume, we construct a *TNB* coordinate system (i.e. Frenet frame) based on the centre point $S(s_0)$ of the sub-skeleton. Let T, N, B be the unit vectors representing the tangent, normal, and binormal of the curve skeleton at $s = s_0$, then these vectors collectively form an orthonormal basis of 3-D space with coordinate origin at $S(s_0)$.
4) Sample the shape control points from the tubular surface section contained within the AABB.
   To identify the surface point, the coordinates of the voxel points in this AABB volume are transformed into the *TNB* coordinate space.
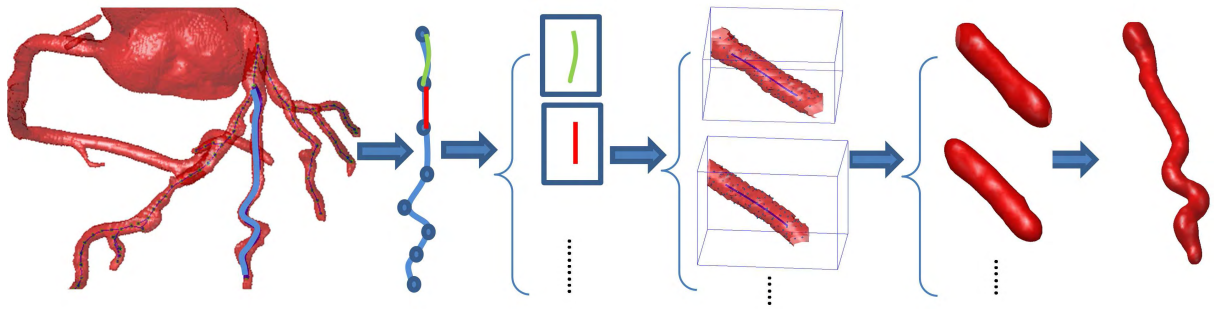   After the process of segmentation, the shape of vessel can be identified as the voxels with gray value ≥ 0,

FIGURE 4. The pipeline of the proposed method for the accurate geometry reconstruction of coronary arteries.
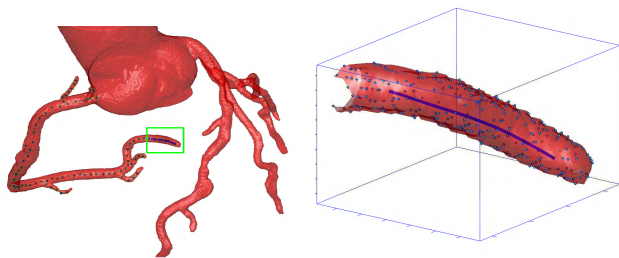

FIGURE 5. A sub-skeleton subdivided from the whole skeleton(left), and the corresponding axis-aligned bounding box(right).

which can be conveniently extracted as the control points of the vessel surface.

These extracted surface points are expressed in the *TNB* coordinates, as the extraction process is performed under the local *TNB* coordinates system.

5) Substitute the *TNB* coordinates of the extract control points into the formula (1) to build from the point cloud an implicit surface((see step (3) in subsection III.A), which is transformed to R^3 space by mapping 3-D Space R^3 to *TNB* coordinate system. An implicit surface will be obtained at this stage for each AABB.

6) Employ Smooth Piecewise Polynomial Blending Operator (SPPBO) to blend different implicitly-defined vascular segments to form a complete vessel branch, according to formula (4).

7) Continue to employ SPPBO to blend different vessel branches together to construct the complete vascular tree.(see Fig.6)
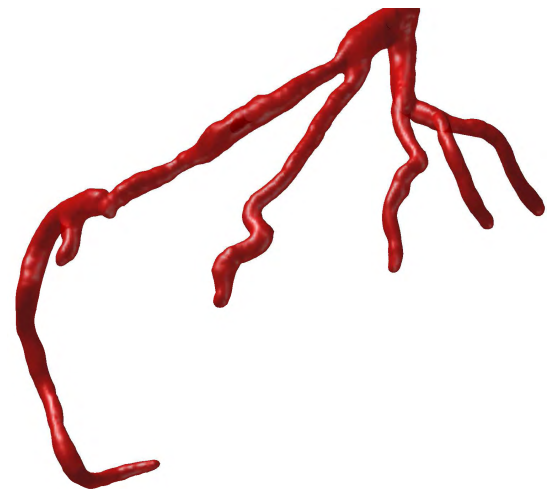
C. FURTHER IMPLEMENTATION DETAILS

One crucial issue with implicit modeling is how to subdivide the point cloud such that each parts well-described using the model. In the proposed method, we choose to subdivide the data set from the tubular surface section contained within its corresponding AABB. It works in most cases for tree-like shape modeling. However, as the topology of vascular structure is very intricate, and the vessel branch could be very tortuous, the subdivision method may not work in some cases. As shown in Fig.7, left is the full view of a vascular tree, and middle is the detail look at a very tortuous vessel
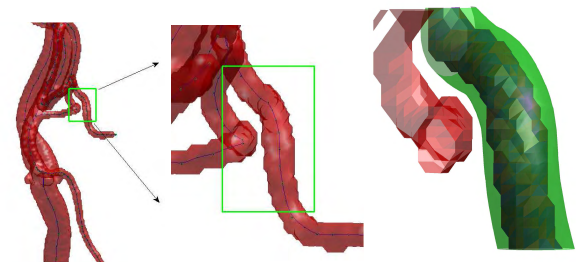

FIGURE 6. The reconstructed result of a left coronary artery with the proposed method.

FIGURE 7. Illustration on the utilizing of a cylindrical mask to discard the unintended parts inside the AABB: The full view of a vascular tree (left), and the detail look at a very tortuous vessel branch (middle), as well as the cylindrical mask along the subdivided skeleton (right). Green rectangle represents the AABB containing the subdivided segment considered for modeling, and green cylinder represents the cylindrical mask containing the tubular surface section for data cloud subdivision.

branch. Green rectangle represents the AABB area containing the subdivided segment considered for modeling. Due to the high tortuosity of the vessel branch, some unintended parts are inside the AABB, which can lead to unsatisfied modeling result (see Fig.8 (left)). In order to solve this problem, we add a cylindrical mask along the subdivided skeleton (see the green cylinder in Fig.7 (right)). Only the tubular surface section inside the cylindrical mask is considered for
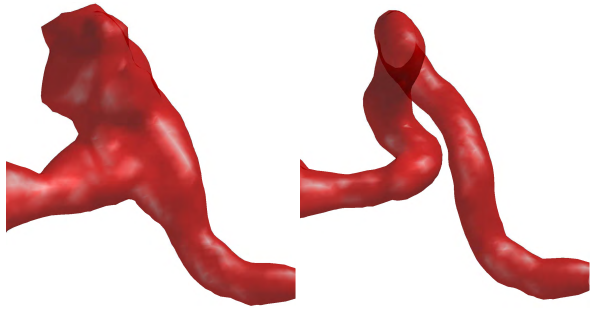
FIGURE 8. The modeling result of highly tortuous vessel branch: The unsatisfied result (left), and the satisfied result by using a cylindrical mask (right).

data cloud subdivision. With this cylindrical mask, we can achieve satisfied modeling result for even highly tortuous vessel branch (see Fig.8 (right)).

IV. RESULTS AND DISCUSSION

### A. ALGORITHM PARAMETER CONFIGURATION

In the proposed algorithms, a few parameters are used, and the way these parameters are configured will affect the fitting results. In the algorithm, parameters n and δ are used in SPPBO for shape blending. In SPPBO, n is an integer parameter and is used to specify the degree of smoothness of the blending operator. Larger n values define higher degree of smoothness blending operators, but has a higher computational cost. δ in SPPBO is used to control to what extent the original shapes involved in the blending operation need to be preserved. Smaller δ values indicate that more portion of original shapes are to be preserved. When δ tends to 0, the corresponding blending operator becomes $\max(x, y)$ or $\min(x, y)$. Thus, when δ is set too small, SPPBO will behave like $\max(x, y)$ or $\min(x, y)$, and the combined surface may not be joined smoothly as real blood vessels. For more detailed discussion on the setting of the parameters n and δ, please refer to [7]. The modeling results of the proposed algorithm are affected by the length of the subdivided skeleton segment l_s. In general, the length of each subdivided skeleton segment should not be too long. This is because if the subdivided skeleton segment is too long, the fitting results may not be satisfactory, especially when the curvature of the skeleton is high. Some in-depth investigations to the fitting effect concerning different skeleton segment lengths will be given in the next subsection. The detailed descriptions to the parameter values used in our experiments are summarized in Table 1.
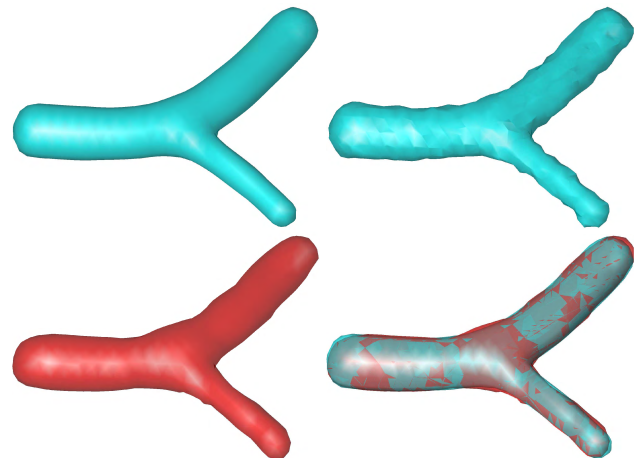
B. SYNTHETIC EXPERIMENT

Two typical synthetic shapes are used for the first test of the proposed method. As shown in Fig.9 and Fig.10, one is a "M" shape (M) with the resolution of $81 \times 81 \times 21$, and the other is a bifurcation (B) with the resolution of $51 \times 51 \times 21$. The original shapes are corrupted by zero-mean Gaussian noise with variances of 0.001 to simulate real medical data. Sub-figures (bottom left) present the modeling results using

TABLE 1. Parameter descriptions and values for the proposed algorithms.

| Name	Description	Value
n_t	Smoothness degree in SPPBO to form tubular shape	2
δ_t	Blending range-control parameter in SPPBO to form tubular shape	0.2
n_b	Smoothness degree in SPPBO to blend different branches into a tree structure	2
δ_b	Blending range-control parameter in SPPBO to blend different branches into a tree structure	0.4
l_s	The length of the subdivided skeleton segment (indicated by the number of the interpolated-spline points of the parametric skeleton $S(s)$)	[100,900]
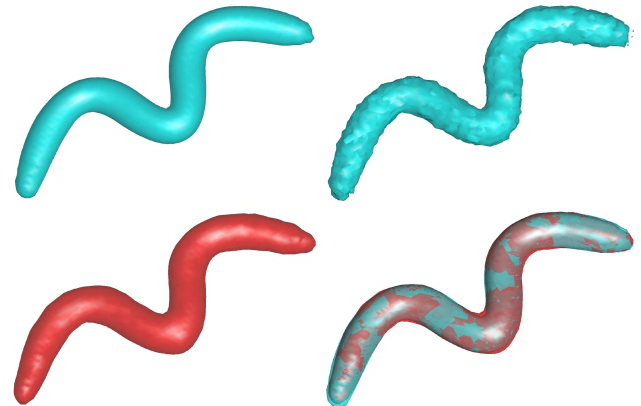
FIGURE 9. The experiment on the synthetic "M" shape: The iso-surface of the original "M" shape(top left), the iso-surface of corrupted data by Gaussian noise distributions with variances of 0.001 (top right), the modeling result using the proposed method based on the control points extracted from the corrupted data (bottom left), direct visual comparison of the iso-surfaces between the modeling results and the original shapes (bottom right).

FIGURE 10. The experiment on the synthetic bifurcation shape: The iso-surface of the original bifurcation shape(top left),the iso-surface of corrupted data by Gaussian noise distributions with variances of 0.001 (top right), the modeling result using the proposed method based on the control points extracted from the corrupted data (bottom left), direct visual comparison of the iso-surfaces between the modeling results and the original shapes (bottom right).

the proposed method based on the control points extracted from the corrupted data, which shows that the proposed technique can achieve satisfactory modeling results and produce high visual quality for very curved shape and bifurcation.
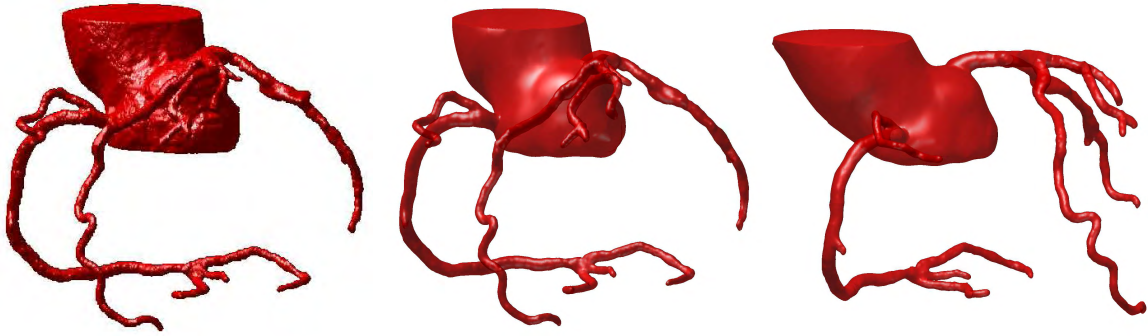
FIGURE 11. Geometric reconstruction of coronary arteries: The isosurface rendering of segmentation result using level-set method (left), and the reconstruction results using the proposed method (middle and right).

In addition, Sub-figures (bottom right) present the direct visual comparison between the iso-surfaces of the modeling results and the original shapes. As can be seen from the figures, there is high overlapping between the two iso-surfaces, even though the modeling shapes were reconstructed from the corrupted data, which illustrates that the proposed method has the ability to faithfully model the original shapes even with corrupted noises.

Besides the above visual inspection, we also conduct a quantitative analysis to judge whether the underly data are faithfully represented. For judging the accuracy, we calculate the Euclidean distances between the iso-surfaces of the modeling results and the original synthetic shapes. The following statistical measures are calculated: median of the distance (Med), root mean square distance (Rms), minimum distance (Min), and maximum distance (Max). We describe the deviation in relation to the resolution of the test dataset, i.e., length of the voxel diagonal (voxDiag) [25]. For estimating the smoothness, we examine the median of the unsigned mean curvatures (MUMC) [35] for all vertices on the modeled surface. In order to investigate the fitting effect concerning different skeleton segment lengths, we calculate the above statistical measures based on the modeling results with different l_s. Table 2 reports the quantitative analysis results with the calculated statistical measures. Excellent distance figures were recorded for the both synthetic datasets. For all the tests, Med, Rms, and Min deviations are much less than half of the length of the voxel diagonal (voxDiag), and even the Max deviations are not bigger than 0.8 times voxDiag. For the ''M'' shape dataset, it could be observed that the lowest deviations (Med: 0.09, Rms: 0.16, Min: 0, Max: 0.55) occur when the l_s value is set as 300. For the bifurcation shape dataset, the measured lowest deviations are even smaller (Med: 0.06, Rms: 0.10, Min: 0, Max: 0.48), which can be obtained when the l_s value is set as 500. It makes sense that the lowest deviations can be obtained with a longer subdivided skeleton segment for the second dataset, since the skeleton curvature of the bifurcation shape is much smaller than that of the ''M'' shape. In addition, the modelled surfaces are reconstructed with quite satisfied smoothness, not only in visual inspection but also the quantitative analysis

TABLE 2. Quantitative analysis for judging the accuracy and smoothness of the proposed method based on the synthetic datasets. Distance values are related to *voxDiag*. The accuracy is measured by calculating the Euclidean distances between the iso-surfaces of the modeling results and the original synthetic shapes, and the smoothness is estimated by measuring the MUMC of the reconstructed surface. The statistical measures are calculated based on the modeling results with different l_s.

Data sets	l_s	Euclidean Distance				MUMC
		Med	Rms	Min	Max	
M	100	0.14	0.19	0	0.65	0.15
	200	0.10	0.17	0	0.70	0.16
	300	0.09	0.16	0	0.55	0.16
	400	0.09	0.16	0	0.70	0.16
	500	0.09	0.16	0	0.65	0.17
	600	0.10	0.17	0	0.70	0.17
	700	0.10	0.16	0	0.70	0.17
B	100	0.11	0.17	0	0.80	0.23
	200	0.09	0.13	0	0.49	0.24
	300	0.09	0.14	0	0.48	0.25
	400	0.08	0.13	0	0.48	0.25
	500	0.06	0.10	0	0.48	0.25
	600	0.07	0.10	0	0.48	0.25
	700	0.07	0.10	0	0.48	0.25
	800	0.07	0.14	0	0.48	0.26
	900	0.09	0.21	0	0.70	0.26

(the MUMC is generally as small as 0.16 for the ''M'' shape and 0.25 for the bifurcation shape).

C. EXPERIMENTS ON VASCULAR DATASETS
The proposed methods have been applied to 12 medical datasets for the geometric reconstruction of coronary arteries. A typical example is presented below, which is the reconstruction of coronary arteries from the 3-D CT angiography (CTA) images with a resolution of $512 \times 512 \times 299$ and spacing of $0.3906\ mm \times 0.3906\ mm \times 0.5\ mm$. Fig.11(left) is the isosurface rendering of segmentation result using level set method, which suffers from aliasing artifacts and diverges considerably from the real vessels. On the other hand, as can be seen from Fig.11(middle and left), both left and right coronary trees are successfully reconstructed from the 3-D CTA dataset. Very curved and complex structures can be reconstructed faithfully using our method, which can achieve superior visual quality and produce smooth transitions at branchings.

FIGURE 12. Two typical modeling results of other vascular structures based on the proposed method: MRA cerebral vasculatures (left); CTA carotid arteries (right).

The developed implicit modeling techniques can be also applied to the reconstruction of vascular geometry for the other parts of the vascular system. Fig.12 presents two typical modeling results of other vascular structures based on the proposed method. One is the geometry modeling of cerebral vasculatures for the 3-D magnetic resonance angiography (MRA) images, and the other is the geometry modeling of carotid arteries for the 3-D CT angiography (CTA) images. As shown in the figures, the proposed method can correctly and faithfully represent the morphology and topology of vascular structures, even for very thin and curved branches.

D. COMPARISON WITH THE PAS BASED TECHNIQUE

There are two main differences between the proposed method and PAS based technique, which can achieve vascular models with extremely high quality. First and foremost, the proposed modeling technique is a one-step fitting based on solving a general eigen-system, which can directly reconstruct 3-D geometric shapes from the point cloud extracted from vascular surfaces. As shown in Fig.13, top left is the segmentation result of a section of vessel branch, in which the cyan points represent the extracted surface points for geometry reconstruction, and top right is the reconstruction result based on the control points using the proposed method. On the other hand, the technique based on PAS needs two steps to reconstruct the 3-D geometric shapes of vasculatures. Firstly, the vessel cross sections are specified using the 2-D PAS, and then, different cross-section profiles are weighted and summed up along the skeleton using the partial shape preserving (PSP) spline basis functions [36] to form the 3-D geometric shapes (see Fig.13(bottom left and bottom right)). Compared with the PAS based technique, the presented method is more efficient and compact, and can achieve more faithful and accurate vessel surfaces than PAS method does.

In PAS method, a cross-section specific vascular segmentation algorithm has to be used as the vascular surface is constructed cross-section by cross-section along the vascular vessel, whereas the RBFEC method allows to use any segmentation algorithm to extract the points from the vascular surface. In addition, RBFEC is a surface interpolation technique, which can produce an implicit surface interpolating the given control points (see Fig.13(top right)); while the
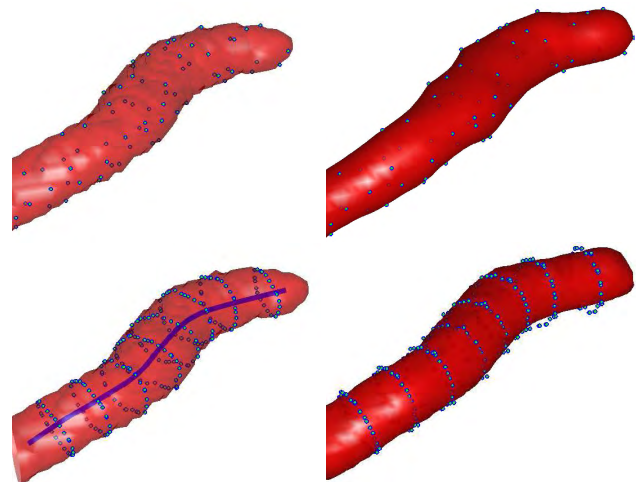
FIGURE 13. The comparison between PAS method and our method: The segmentation result of a section of vessel branch with extracted surface points for reconstruction (top left), the reconstruction result based on the control points using the proposed method (top right), the extracted contour points of different vessel cross sections along the skeleton (bottom left), the reconstruction result based on the cross-section profiles using PAS method (bottom right).

PAS method is only an approximation to the actual vascular surface captured by the control points (see Fig.13(bottom right)). That is, RBFEC based technique can reconstruct the vessel surface more accurately than 2-D PAS technique does.

E. QUANTITATIVE VALIDATION

As we known, the accuracy and smoothness of vascular geometry reconstruction from segmentations need to be traded off in a certain level. However, an excellent technique should be able to generate vascular geometry as accurate as possible with certain smoothness. To validate the proposed method on the geometry modeling of coronary arteries, we conduct a quantitative analysis based on the experiments of the 12 medical datasets. For judging the accuracy, we calculate the Euclidean distance between the segmented data and the modeled vascular surfaces, as there is no ground truth on actual vascular anatomy. For estimating the smoothness, we examine the median of the unsigned mean curvatures (MUMC) [35] for all vertices on the modeled surface.

Table 3 presents the quantitative analysis results with the calculated statistical measures based on the 12 coronary artery datasets. The median distances are no larger than 0.15mm for all the experimental datasets, which is a fraction of the voxel size of current CT imaging. The root mean square distance (Rms) is generally as small as 0.20mm, which is below half of voxDiag for each considered dataset. Even the max deviations are not higher than 2mm, which generally occurs at the areas close to the ends of the vessel tree. In addition, the measured MUMC of each considered dataset is no larger than 0.17, which means the proposed method can achieve smooth modeled surface of high quality.

We also conduct the direct quantitative comparisons between the proposed method and other methods for the

TABLE 3. Quantitative analysis for judging the accuracy and smoothness of the proposed method based on the 12 coronary artery datasets. The accuracy is measured by calculating the Euclidean distances (in millimeters) between the iso-surfaces of the modeling results and the segmented results, and the smoothness is estimated by measuring the MUMC of the reconstructed surface. The statistical measures are calculated based on the modeling results with $l_s = 300$.

Data sets	Euclidean Distance				MUMC
	Med	Rms	Min	Max	
Data 1	0.10	0.32	0	1.56	0.15
Data 2	0.10	0.30	0	1.70	0.12
Data 3	0.12	0.20	0	1.14	0.16
Data 4	0.12	0.22	0	1.29	0.16
Data 5	0.11	0.20	0	1.15	0.15
Data 6	0.14	0.27	0	1.46	0.15
Data 7	0.11	0.20	0	1.54	0.17
Data 8	0.11	0.19	0	1.15	0.15
Data 9	0.13	0.22	0	1.45	0.16
Data 10	0.13	0.22	0	1.57	0.17
Data 11	0.12	0.21	0	1.33	0.15
Data 12	0.12	0.20	0	1.09	0.15

TABLE 4. Quantitative comparison between our proposed method and the MPUI based method and the PAS based method for the geometry reconstruction of coronary arteries based on the 12 coronary artery datasets. Distance values are in millimeters.

Methods	Distance		MUMC
	Med	Rms	
MPUI based method	0.22	0.26	0.19
PAS based method	0.15	0.24	0.15
The proposed method	0.12	0.23	0.15

geometry reconstruction of coronary arteries. The presented values are the average of the above 12 experimental datasets. As shown in Table 4, the averaged Med and Rms values corresponding to the models built from our method are only 0.12mm and 0.23mm, which are both smaller than that based on the MPUI method and PAS method. The averaged MUMC value of our built models is as small as that based on PAS method, which is regarded as an excellent approach to reconstruct vessel tree with great smoothness property [33]. The quantitative analysis demonstrates the proposed method can achieve more accurate vessel models than the other two methods.

F. COMPUTATIONAL COMPLEXITY

The computational cost of the proposed method mainly depends on the complexity of the vascular tree and the resolution of input dataset. Table 5 presents the information concerning the complexity of the resulting models and the reconstruction times based on the first example of experimental dataset (Fig. 11). The reconstruction time includes the time of point extraction, construction of implicit functions, evaluation of scalar values, and generation of patch faces. As can be seen from the table, the proposed method is nearly three times faster than PAS based method.

V. CONCLUSION AND FUTURE WORK

In this paper, a new implicit modeling technique has been proposed and applied to the geometric reconstruction of patient-specific coronary arteries. Compared to the LIM method [34], the proposed technique is not only much simpler but more

TABLE 5. Performance measurements of the proposed method and PAS based method for the implicit surface reconstruction of coronary artery trees carried out on an Intel Core i5 CPU with two cores @3.2GHz and 8GB RAM. The reconstruction time is measured in seconds.

Data sets	PAS based method		The proposed method	
	Face number	Time(sec)	Face number	Time(sec)
LCT	44696	53.70	50668	23.17
RCT	35556	46.86	40776	18.27

direct to fit an implicit surface to the point cloud extracted from a complex vascular surface. With the proposed implicit modeling method, faithful and smooth coronary models can be reconstructed from given segmented CTA datasets. The experimental results and validations have demonstrated that our methods can reconstruct the geometry of coronary arteries with high accuracy and smoothness.

The developed technique is generalizable to other application areas, which can be applied to the reconstruction of vascular geometry for the other parts of the vascular system. The main improvement with our proposed technique lies in its simplicity and the degree of fitting accuracy. The proposed modeling technique is a one-step fitting based on solving a general eigen-system, which can directly reconstruct with high precision the 3-D geometric shapes of vascular surface from the point cloud extracted from the vascular surface segments. In addition, our RBFEC based technique can specify the vessel surface more accurately than 2-D PAS technique does, as it can construct an interpolating implicit surface that goes through all the control points.

One of our future work is to employ the NVIDIA Compute Unified Device Architecture(CUDA) for the parallel computation in modern graphics hardware, which can greatly reduce the reconstruction time and may process even at interactive frame rates.

REFERENCES

[1] V. Roger *et al.*, "Heart disease and stroke statistics—2012 update: A report from the American Heart Association," *Circulation*, vol. 125, no. 1, pp. e12–e230, 2012.

[2] V. Gorenoi, M. P. Schönermark, and A. Hagen, "CT coronary angiography vs. invasive coronary angiography in CHD," *GMS Health Technol. Assessment*, vol. 8, Apr. 2012.

[3] S. Windecker, W. Maier-Rudolph, T. Bonzel, G. Heyndrickx, J. M. Lablanche, M. C. Morice, V. Muhlberger, K. L. Neuhaus, F. Piscione, M. Van D. Brand, W. Wijns, and B. Meier, "Interventional cardiology in Europe 1995," *Eur. Heart J.*, vol. 20, no. 7, pp. 484–495, 1999.

[4] G. Xiong, G. Choi, and C. A. Taylor, "Virtual interventions for image-based blood flow computation," *Comput.-Aided Des.*, vol. 44, pp. 3–14, Jan. 2012.

[5] C. A. Taylor, T. A. Fonte, and J. K. Min, "Computational fluid dynamics applied to cardiac computed tomography for noninvasive quantification of fractional flow reserve: Scientific basis," *J. Amer. College Cardiol.*, vol. 61, no. 22, pp. 2233–2241, 2013.

[6] Q. Li, D. Wills, R. Phillips, W. J. Viant, J. G. Griffiths, and J. Ward, "Implicit fitting using radial basis functions with ellipsoid constraint," *Comput. Graph. Forum*, vol. 23, no. 1, pp. 55–69, 2004.

[7] Q. Li, "Smooth piecewise polynomial blending operations for implicit shapes," *Comput. Graph. Forum*, vol. 26, no. 2, pp. 157–171, 2007.

[8] D. Lesage, E. D. Angelini, I. Bloch, and G. Funka-Lea, "A review of 3D vessel lumen segmentation techniques: Models, features and extraction schemes," *Med. Image Anal.*, vol. 13, no. 6, pp. 819–845, Aug. 2009.

[9] Z. Zhang, H. Li, X. Chen, D. Yu, Z. Jia, K. Pu, and X. Wang, "3D segmentation of coronary arteries based on probabilistic decision and region growing," *J. Tianjin Univ.*, vol. 44, no. 5, pp. 454–457, 2011.

[10] C. Zhou, H.-P. Chan, A. Chughtai, S. Patel, L. M. Hadjiiski, J. Wei, and E. A. Kazerooni, "Automated coronary artery tree extraction in coronary CT angiography using a multiscale enhancement and dynamic balloon tracking (MSCAR-DBT) method," *Comput. Med. Imag. Graph.*, vol. 36, no. 1, pp. 1–10, 2012.

[11] F. Lugauer, J. Zhang, Y. Zheng, J. Hornegger, and B. M. Kelm, "Improving accuracy in coronary lumen segmentation via explicit calcium exclusion, learning-based ray detection and surface optimization," *Proc. SPIE Med. Imag. Image Process.*, vol. 9034, p. 90343U, Mar. 2014.

[12] F. Lugauer, Y. Zheng, J. Hornegger, and B. M. Kelm, *Precise Lumen Segmentation Coronary Computed Tomography Angiography* (Lecture Notes in Computer Science). Cambridge, MA, USA: Springer, 2014, ch. 13, pp. 137–147.

[13] H. K. Hahn, B. Preim, D. Selle, and H. Peitgen, "Visualization and interaction techniques for the exploration of vascular structures," in *Proc. IEEE Vis.*, Oct. 2001, pp. 395–578.

[14] Y. Masutani, K. Masamune, and T. Dohi, "Region-growing based feature extraction algorithm for tree-like objects," in *Proc. Int. Conf. Vis. Biomed. Comput.*, 1996, pp. 159–171.

[15] P. Felkel, R. Wegenkitt, and K. Buhler, "Surface models of tube trees," in *Proc. Comput. Graph. Int.*, Jun. 2004, pp. 70–77.

[16] B. Alexander, R. Bernhard, and B. Reinhard, "Reconstruction and representation of tubular structures using simplex meshes," in *Proc. Winter School Comput. Graph. (WSCG)*, 2005, pp. 61–64.

[17] X. Wu, V. Luboz, K. Krissian, S. Cotin, and S. Dawson, "Segmentation and reconstruction of vascular structures for 3D real-time simulation," *Med. Image Anal.*, vol. 15, no. 1, pp. 22–34, 2011.

[18] X. Wang, Z. Wu, J. Shen, T. Zhang, X. Mou, and M. Zhou, "Repairing the cerebral vascular through blending ball B-Spline curves with G2 continuity," *Neurocomputing*, vol. 173, pp. 768–777, Jan. 2016.

[19] J. Bloomenthal, "Skeletal design of natural forms," Ph.D. dissertation, Dept. Comput. Sci., Univ. Calgary, Calgary, AB, Canada, 1995.

[20] L. Barthe, N. A. Dodgson, M. A. Sabin, B. Wyvill, and V. Gaildrat, "Two-dimensional potential fields for advanced implicit modeling operators," *Comput. Graph. Forum*, vol. 22, no. 1, pp. 23–33, 2003.

[21] M. Lin and S. Gottschalk, "Collision detection between geometric models: A survey," in *Proc. IMA Conf. Math. Surf.*, 1998, pp. 602–608.

[22] S. Oeltze and B. Preim, "Visualization of vasculature with convolution surfaces: Method, validation and evaluation," *IEEE Trans. Med. Imag.*, vol. 24, no. 4, pp. 540–548, Apr. 2005.

[23] J. Bloomenthal and K. Shoemake, "Convolution surfaces," *Comput. Graph.*, vol. 25, no. 4, pp. 251–256, 1991.

[24] C. Schumann, S. Oeltze, R. Bade, B. Preim, and H.-O. Peitgen, "Model-free surface visualization of vascular trees," in *Proc. IEEE VGTC Conf. Vis.*, May 2007, pp. 283–290.

[25] C. Schumann, M. Neugebauer, R. Bade, B. Preim, and H.-O. Peitgen, "Implicit vessel surface reconstruction for visualization and CFD simulation," *Int. J. Comput. Assist. Radiol. Surg.*, vol. 2, no. 5, pp. 275–286, 2008.

[26] Y. Ohtake, A. Belyaev, M. Alexa, G. Turk, and H.-P. Seidel, "Multi-level partition of unity implicits," *ACM Trans. Graph.*, vol. 22, no. 3, pp. 463–470, 2003.

[27] J. Wu, M. Wei, Y. Li, X. Ma, F. Jia, and Q. Hu, "Scale-adaptive surface modeling of vascular structures," *Biomed. Eng. OnLine*, vol. 9, no. 1, p. 75, 2010.

[28] Q. Hong, Q. Li, and J. Tian, "Implicit reconstruction of vasculatures using bivariate piecewise algebraic splines," *IEEE Trans. Med. Imag.*, vol. 31, no. 3, pp. 543–553, Mar. 2012.

[29] Q. Hong, "A skeleton-based technique for modelling implicit surfaces," in *Proc. 6th Int. Congr. Image Signal Process. (CISP)*, Dec. 2013, pp. 686–691.

[30] Q. Hong, Y. Li, Q. Li, B. Wang, J. Yao, Q. Wu, and Y. She, "An implicit skeleton-based method for the geometry reconstruction of vasculatures," *Vis. Comput.*, vol. 32, no. 10, pp. 1251–1262, 2016.

[31] Q. Hong, Q. Li, B. Wang, K. Liu, F. Lin, J. Lin, X. Cheng, Z. Zhang, and M. Zeng, "Accurate geometry modeling of vasculatures using implicit fitting with 2D radial basis functions," *Comput. Aided Geometric Design*, vol. 62, pp. 206–216, May 2018.

[32] Q. Li and J. Tian, "2D piecewise algebraic splines for implicit modeling," *ACM Trans. Graph.*, vol. 28, no. 2, p. 13, 2009.

[33] J. Kretschmer, C. Godenschwager, B. Preim, and M. Stamminger, "Interactive patient-specific vascular modeling with sweep surfaces," *IEEE Trans. Vis. Comput. Graphics*, vol. 19, no. 12, pp. 2828–2837, Dec. 2013.

[34] E. Kerrien, A. Yureidini, J. Dequidt, C. Duriez, R. Anxionnat, and S. Cotin, "Blood vessel modeling for interactive simulation of interventional neuroradiology procedures," *Med. Image Anal.*, vol. 35, pp. 685–698, Jan. 2017.

[35] D. Chen-shi and W. Guo-zhao, "Curvatures estimation on triangular mesh," *J. Zhejiang Univ.-Sci. A*, vol. 6, pp. 128–136, Aug. 2005.

[36] Q. Li and J. Tian, "Partial shape-preserving splines," *Comput.-Aided Des.*, vol. 43, no. 4, pp. 394–409, 2011.
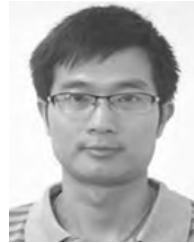
QINGQI HONG received the Ph.D. degree in computer science from the University of Hull, U.K. He is currently an Associate Professor with the Software School, Xiamen University, China. His current research interests include medical imaging processing, 3D visualization, 3D modeling, computer-aided diagnosis and surgery, deep learning, and GPU computing.

QINGDE LI received the Ph.D. degree in computer science from the University of Hull, U.K., where he is currently a Lecturer with the Department of Computer Science. His current research interests include computer graphics, medical image processing, and geometric modeling.

BEIZHAN WANG received the Ph.D. degree in computer science from Northwest Polytechnical University, China. He is currently a Professor with the Software School, Xiamen University, China. His current research interests include data warehouse, data mining, and software architecture.

KUNHONG LIU received the Ph.D. degree from the University of Science and Technology of China. He is currently a Professor with the Software School, Xiamen University, China. His current research interests include data mining, machine learning, and intelligence analysis.

QUAN QI received the Ph.D. degree in computer science from the University of Hull, U.K. He is currently a Lecturer with the College of Information Science and Technology, Shihezi University, China. His research interests include computer graphics, medical image processing, and geometric modeling.

• • •